Journal of Power Sources 268 (2014) 261–268

Contents lists available at ScienceDirect

Journal of Power Sources

journal homepage: www.elsevier.com/locate/jpowsour

# Peak power prediction of a vanadium redox flow battery

V.K. Yu*, D. Chen

*Department of Mechanical Engineering, The University of Texas at Austin, 1 University Station C2200, Austin, TX 78712, USA*

## HIGHLIGHTS

- We devise a control strategy to maximize battery life during discharge.
- We model a VRFB system to predict the peak power.
- The model considers voltage and pump losses when calculating peak power.
- The model accounts for mass transfer effect and non-uniform vanadium concentration.
- Electrode porosity, temperature, and vanadium concentration affect peak power.

## ARTICLE INFO

*Article history:*
Received 16 January 2014
Received in revised form
30 April 2014
Accepted 9 June 2014
Available online 18 June 2014

*Keywords:*
Flow battery
Vanadium
Energy storage
Modeling

## ABSTRACT

The vanadium redox flow battery (VRFB) is a promising grid-scale energy storage technology, but future widespread commercialization requires a considerable reduction in capital costs. Determining the appropriate battery size for the intended power range can help minimize the amount of materials needed, thereby reducing capital costs. A physics-based model is an essential tool for predicting the power range of large scale VRFB systems to aid in the design optimization process. This paper presents a modeling framework that accounts for the effects of flow rate on the pumping losses, local mass transfer rate, and nonuniform vanadium concentration in the cell. The resulting low-order model captures battery performance accurately even at high power densities and remains computationally practical for stack-level optimization and control purposes. We first use the model to devise an optimal control strategy that maximizes battery life during discharge. Assuming optimal control is implemented, we then determine the upper efficiency limits of a given VRFB system and compare the net power and associated overpotential and pumping losses at different operating points. We also investigate the effects of varying the electrode porosity, stack temperature, and total vanadium concentration on the peak power.



## 1. Introduction

With the rapid increase of grid-connected intermittent renewable sources such as wind and solar energy, it is becoming crucial to have a reliable and efficient means of electrical energy storage that can maintain stable power output and high power quality. Among existing technologies, the vanadium redox flow battery (VRFB) is one of the most promising solutions for grid-level energy storage because of its fast response rate and high efficiency [1]. Furthermore, VRFBs are modular so they can easily scale to meet a wide range of power and capacity requirements by increasing the number of cells in the stack and electrolyte volume, respectively. Still, VRFBs are too expensive to be commercially viable [2].

Operating costs can be reduced by improving the performance and efficiency of VRFBs. To achieve this objective, researchers are designing better materials [3] and cell architectures [4] as well as developing physics-based VRFB models with varying levels of complexity. Shah et al. [5–8] developed first principle models, incorporating fundamental conservation laws and electrode kinetics, capable of predicting 2-D distributions of concentration, overpotential, and current density in a unit cell for a range of operating conditions. Xu et al. [9] developed a 3-D model for investigating different flow field designs to reduce overpotential losses in a single cell. These high fidelity models are valuable for improving our understanding of the important physical phenomena that affect cell performance and efficiency. Nonetheless, Kear et al. [10] emphasized the additional need for practical stack-level

* Corresponding author. Tel.: +1 5124714487; fax: +1 5124718727.
*E-mail addresses:* victory118@utexas.edu (V.K. Yu), dmchen@me.utexas.edu (D. Chen).

http://dx.doi.org/10.1016/j.jpowsour.2014.06.053
0378-7753/

models that can help in optimizing the design of large-scale systems.

This need was further validated through an economic study by Hittinger et al. [11], who showed that improvements in capital cost and power limit, rather than efficiency and operating cost, have the greatest potential impact on the profitability of modular battery storage technologies for load following and frequency regulation applications. Indeed, optimal battery sizing can help minimize the amount of materials needed for the intended power requirement, resulting in lower capital costs. For this reason, there is a strong incentive to pursue research not only in engineering new materials to operate at higher power densities, but also in developing modeling and simulation tools to predict the peak power of VRFB systems so that their full operating range can be utilized [12]. Ma et al. [13] conducted experiments to characterize the performance of a specific VRFB system and devised a flow rate strategy to improve system efficiency at various states of charge (SOC). Xiong et al. [14] took a more general approach by developing a lumped parameter model, accounting for temperature effects and pumping losses, to predict the optimal flow rate that maximizes system efficiency under different operating conditions and SOC. Although this model is computationally practical for stack-level optimization and control purposes, it lacks sufficient detail in the voltage model to predict battery performance accurately when operating at high power densities.

In this paper, we present a modeling framework that accounts for the effects of flow rate on the pumping losses, local mass transfer rate, and nonuniform vanadium concentration in the cell. A sufficiently high flow rate is desirable for increasing the local mass transfer rate, thereby reducing the concentration overpotential. However, an optimal flow rate strategy should consider the trade-off between reducing overpotential and using excessive pump power. A quantitative assessment is provided in this paper to better understand the trade-off between these two competing objectives in order to come up with an optimal flow rate strategy. Depending on the flow rate and reaction rate, a lumped parameter model may give an unsatisfactory approximation of the bulk vanadium concentration inside the cell. To improve the accuracy of the lumped model with minimal increase in computational cost, we assume a linear profile for the vanadium concentration along cell length and calculate an average open circuit voltage and overpotential. The resulting low-order model includes sufficient detail to capture the internal battery losses at high power densities while remaining practical for stack-level optimization and control purposes. First we use our model to devise an optimal control strategy that maximizes battery life during discharge over a range of SOC and power demand. Assuming optimal control is implemented, we then determine the upper efficiency limits of the given VRFB system design. The net power and associated overpotential and pumping losses are compared quantitatively at different operating points. To further extend the analysis, we investigate the effects of varying important design parameters including the electrode porosity, stack temperature, and total vanadium concentration on the peak power. During the initial design stage, these insights can help size a VRFB system appropriately for the intended power range while minimizing capital costs.

## 2. Methodology

We consider a VRFB system as shown in Fig. 1. The net power output of a VRFB system is the sum of the stack power minus the power consumed by auxiliary components such as the pump, power electronics, thermal management system, and control system. In our analysis, we only consider the internal battery overpotential and pumping losses whereas power consumed by all other auxiliary components is neglected. Pump power has been shown in several pilot experiments to account for a majority of the parasitic

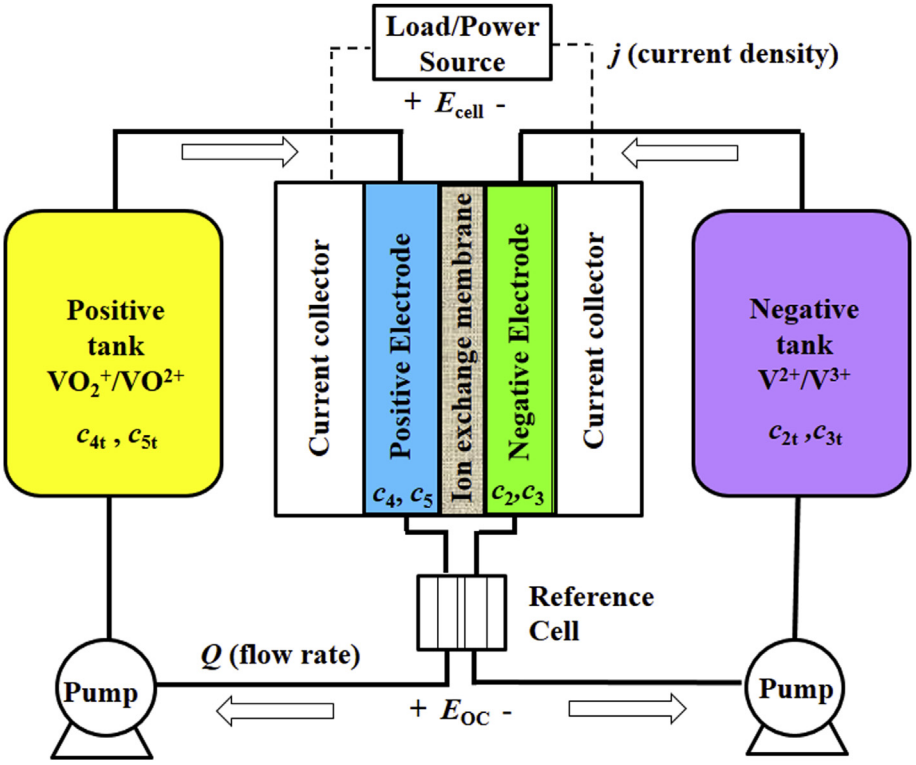


**Fig. 1.** Schematic of a VRFB system.

losses in a VRFB system [1,9,13,16]. Thus, the system net power can be calculated by

$$P_{net} = iE_{OC} - iE_{loss} - P_{pump} \quad (1)$$

where $i$ is the current, $E_{OC}$ is the open circuit voltage, $E_{loss}$ is the internal battery overpotential loss, and $P_{pump}$ is the pump power. The following section explains the derivation of each term in Eq. (1).

### 2.1. Battery model

We first consider the lumped parameter model of a unit cell VRFB system developed by Shah et al. [17] with two major modifications. First, we account for the effect of flow rate on the local mass transfer rate of vanadium ions, which could cause a significant concentration overpotential at high current densities. Second, we use a linear profile to approximate the 1-D vanadium concentration distribution along the cell length and calculate an average open circuit voltage and activation overpotential based on evenly spaced grid points.

Dynamic equations can be obtained by partitioning the unit cell VRFB system into four control volumes and performing a mass balance for each vanadium species. The control volumes include the positive tank, negative tank, positive electrode, and negative electrode. During operation, electrolyte is circulated between the storage tank and the electrode, where electrochemical reactions occur. The electrochemical reactions that occur at the positive and negative electrodes are given by

Positive electrode:

$$VO^{2+} + H_2O \underset{\text{discharge}}{\overset{\text{charge}}{\rightleftharpoons}} VO_2^+ + 2H^+ + e^- \quad (2)$$

Negative electrode:

$$V^{3+} + e^- \underset{\text{discharge}}{\overset{\text{charge}}{\rightleftharpoons}} V^{2+} \quad (3)$$

Thus, the system can be represented by eight state variables in the following state space form:

$$\dot{x}(t) = Ax(t)u_1(t) + Bu_2(t)$$

$$A = \begin{bmatrix} -\frac{1}{\varepsilon V_e} I_{4x4} & \frac{1}{\varepsilon V_e} I_{4x4} \\ \frac{1}{\varepsilon V_{tank}} I_{4x4} & -\frac{1}{\varepsilon V_{tank}} I_{4x4} \end{bmatrix}$$

$$B = \frac{A_m}{\varepsilon V_e F}[-1 \quad 1 \quad 1 \quad -1 \quad 0 \quad 0 \quad 0 \quad 0]^T$$

$$x = [c_2 \quad c_3 \quad c_4 \quad c_5 \quad c_{2t} \quad c_{3t} \quad c_{4t} \quad c_{5t}]^T$$

$$u = [Q \quad j]^T$$

Here, $\varepsilon$ is the electrode porosity, $V_e$ is the electrode volume, $V_{tank}$ is the tank volume, $c_{van}$ is the total vanadium concentration, and $I_{4x4}$ is the identity matrix. The concentrations of $V^{2+}$ and $V^{3+}$ in the negative half-cell and tank are represented by the state variables $c_2$, $c_{2t}$, $c_3$, and $c_{3t}$, respectively. The concentrations of $VO_2^+$ and $VO^{2+}$ in the positive half-cell and tank are represented by the state variables $c_4$, $c_{4t}$, $c_5$, and $c_{5t}$, respectively. The control inputs are the flow rate, $Q$, and current density, $j$. The current density is related to the current by $i = jA_m$, where $A_m$ is the membrane area.

The cell voltage, $E_{cell}$, can be obtained by

$$E_{cell} = E_{OC} - E_{ohm} - |\eta_{pos}| - |\eta_{neg}| \quad (4)$$

where $E_{ohm}$ is the ohmic overpotential and $\eta_{pos}$ and $\eta_{neg}$ are the activation overpotentials at the positive and negative half-cells.

The open circuit voltage can be calculated using the Nernst equation as

$$E_{OC} = E_0^{pos} - E_0^{neg} + \frac{RT}{F}\ln\left(\frac{c_2 c_5 c_{H^+}^2}{c_3 c_4}\right) \quad (5)$$

where $E_0^{pos}$ and $E_0^{neg}$ are the standard reduction potentials for the reactions at the positive and negative half-cells, $R$ is the molar gas constant, $T$ is the stack temperature, $F$ is the Faraday constant, and $c_{H^+}$ is the proton concentration in the positive half-cell. The ohmic overpotential includes losses in the membrane, electrolyte and current collector and is obtained by

$$E_{ohm} = E_m + E_e + E_c \quad (6)$$

Each ohmic overpotential term is calculated respectively by

$$E_m = j\frac{w_m}{\sigma_m} \quad (7)$$

$$E_e = j\frac{w_e}{\varepsilon^{3/2}\sigma_e} \quad (8)$$

$$E_c = j\frac{w_c}{\sigma_c} \quad (9)$$

where $w$ is the width and $\sigma$ is the conductivity. The electrolyte conductivity in Eq. (8) includes a Bruggeman correction to account for the electrode porosity. The membrane conductivity varies as a function of temperature according to the Arrhenius law given by [18]

$$\sigma_m = (0.5139\lambda - 0.326)\exp\left(1268\left[\frac{1}{303} - \frac{1}{T}\right]\right) \quad (10)$$

where the $\lambda$ is membrane water content. The membrane is assumed to be fully saturated with $\lambda = 22$.

The activation overpotential including mass transfer effects can be obtained using the current-overpotential equation given by Ref. [19]

$$\frac{j}{j_0} = \left(1 - \frac{j}{j_{l,c}}\right)\exp\left(-\frac{\alpha F\eta}{RT}\right) - \left(1 - \frac{j}{j_{l,a}}\right)\exp\left(\frac{\alpha F\eta}{RT}\right) \quad (11)$$

where $\alpha$ is the charge transfer coefficient. The exchange current density, $j_0$, is calculated by

Positive electrode:

$$j_{0,pos} = FA_m k_{pos}\sqrt{c_4 c_5} \quad (12)$$

Negative electrode:

$$j_{0,neg} = FA_m k_{neg}\sqrt{c_2 c_3} \quad (13)$$

The reaction rate constants, $k_{pos}$ and $k_{neg}$, vary with temperature according to the Arrhenius law given by

$$k_{pos} = k_{pos}^{ref}\exp\left(\frac{E_a}{R}\left[\frac{1}{T_{ref}} - \frac{1}{T}\right]\right) \quad (14)$$

$k_{neg}$ is found in an analogous manner to Eq. (14). To the best of the authors' knowledge, only the positive activation energy has been reported in literature [23] so it is assumed that the negative activation energy takes on the same value for simulation purposes.

The cathodic and anodic limiting current densities, $j_{l,c}$ and $j_{l,a}$, are the maximum current density limits restricted by the diffusion rate of vanadium species from the bulk solution to the electrode surface and are related to the mass transfer coefficient, $m_{van}$, by

Positive electrode:

$$j_{l,c} = FA_m m_{van} c_5 \tag{15}$$

$$j_{l,a} = -FA_m m_{van} c_4 \tag{16}$$

Negative electrode:

$$j_{l,c} = FA_m m_{van} c_2 \tag{17}$$

$$j_{l,a} = -FA_m m_{van} c_3 \tag{18}$$

All vanadium species are assumed to have the same mass transfer coefficient [15]. The mass transfer coefficient can be related empirically to the electrolyte velocity, $v$, by Ref. [20]

$$m_{van} = 2 \times 10^{-4} v^{0.4} \tag{19}$$

Assuming that the positive and negative sides are completely balanced and neglecting vanadium and water transfer through the membrane, the system can be reduced to two state variables by using a lumped parameter approximation [17]. Accordingly, the SOC in the cell and tank can be defined respectively as

$$SOC_{cell} = \frac{c_2}{c_{van}} = \frac{c_5}{c_{van}} = 1 - \frac{c_3}{c_{van}} = 1 - \frac{c_4}{c_{van}} \tag{20}$$

and

$$SOC_{tank} = \frac{c_{2t}}{c_{van}} = \frac{c_{5t}}{c_{van}} = 1 - \frac{c_{3t}}{c_{van}} = 1 - \frac{c_{4t}}{c_{van}}, \tag{21}$$

Eqs. (5), (11)–(13), and (15)–(18) can be rewritten in terms of the two new state variables, $SOC_{cell}$ and $SOC_{tank}$, by substitution of Eqs. (20) and (21).The resulting system of equations then becomes

$$\dot{x}(t) = Ax(t)u_1(t) + Bu_2(t)$$

$$A = \begin{bmatrix} -\frac{1}{\varepsilon V_e} & \frac{1}{\varepsilon V_e} \\ \frac{1}{\varepsilon V_{tank}} & -\frac{1}{\varepsilon V_{tank}} \end{bmatrix}$$

$$B = \begin{bmatrix} -\frac{A_m}{\varepsilon V_e F c_{van}} & 0 \end{bmatrix}^T$$

$$x = [SOC_{cell} \quad SOC_{tank}]^T$$

$$u = [Q \quad j]^T$$

Because the tank volume is typically much larger than the electrode volume in a utility-scale VRFB system, $SOC_{tank}$ changes much more slowly than $SOC_{cell}$. Assuming that $SOC_{tank}$ remains constant when discharging over a short time interval, the pseudo-steady state value of $SOC_{cell}$ can be calculated for a given $SOC_{tank}$, current, and flow rate by Ref. [21]

$$SOC_{cell} = SOC_{tank} - \frac{jA_m}{QFc_{van}} \tag{22}$$

Eq. (22) can then be used to predict the overpotential loss as a function of $SOC_{tank}$, current, and flow rate. To improve the accuracy of the lumped parameter model, a linear profile can be used to approximate the 1-D SOC distribution along the length of the cell with $SOC_{tank}$ at the cell inlet and $SOC_{cell}$ at the outlet [22]. The SOC at a distance $x$ from the cell inlet can be obtained by

$$SOC_{cell}(x) = SOC_{tank} - \frac{jA_m}{QFc_{van}} \frac{x}{L_e} \tag{23}$$

where $L_e$ is the electrode length in the flow direction. For the simulations in this paper, we use a resolution of $N = 5$ equidistant grid points from $x_1 = 0$ to $x_5 = L_e$ to calculate an average open circuit voltage and overpotential by

$$\overline{E}_{OC} = E_0^{pos} - E_0^{neg} + \frac{2RT}{F}\left(\ln(c_{H^+}) + \frac{1}{N}\sum_{i=1}^{N} \ln\left(\frac{SOC_{cell}(x_i)}{1 - SOC_{cell}(x_i)}\right)\right) \tag{24}$$

and

$$\overline{\eta} = \frac{1}{N}\sum_{i=1}^{N} \eta_i \tag{25}$$

where each $\eta_i$ is a function of $SOC_{cell}(x_i)$ and satisfies Eq. (11).

### 2.2. Pump power model

The pump power required to operate a VRFB system is calculated by

$$P_{pump} = 2\eta_{pump} Q \Delta p_{tot} \tag{26}$$

where $\Delta p_{tot}$ is the total pressure loss, $\eta_{pump} = 0.85$ is the pump efficiency, and the factor of two accounts for the two pumps needed to circulate the positive and negative electrolytes. We use the hydraulic circuit configuration based on a typical VRFB system design presented by Xiong et al. [14] to determine the total pressure loss. In this section, the hydraulic circuit configuration is explained and model equations are summarized. The reader should refer to [14] for more specific details about the hydraulic circuit.

The pressure losses in a VRFB system are comprised of major and minor losses that occur in the cell stack and piping system. The major loss in the cell stack is due to friction in the porous electrode and is calculated by using a modified form of Darcy's equation [5,15]

$$\Delta p_{stack,major} = \frac{\mu v_e L_e}{K} \tag{27}$$

where

$$K = \frac{d_f^2 \varepsilon^3}{16 k_{KC}(1-\varepsilon)^2} \tag{28}$$

Here, $\mu$ is the electrolyte dynamic viscosity, $L_e$ is the electrode length in the flow direction, $A_e = \varepsilon w_e L_e$ is the area normal to the flow, $v_e = Q/A_e$ is the average electrolyte velocity in the electrode, $d_f$ is the mean fiber diameter, and $k_{KC}$ is the Kozeny-Carmen constant. For a cell stack aligned hydraulically in parallel, the pressure drop across each electrode is the same. The major loss in the piping system is due to friction in the pipe walls and is calculated by

$$\Delta p_{pipe,major} = \frac{128 \mu Q L_p}{\pi D_p^4} \tag{29}$$

where $L_p$ is the pipe length and $D_p$ is the pipe diameter.

Based on a typical flow flame design, the minor losses in the cell stack can be approximated by summing the individual minor losses across a series of line and branch flow tees [14]:

$$\Delta p_{\text{stack,minor}} = 2 \times n_{\text{cells}} \left( K_{\text{line}} \rho \frac{v_e^2}{2} + K_{\text{branch}} \rho \frac{v_e^2}{2} \right) \quad (30)$$

Here, $K_{\text{line}} = 0.9$ is the line flow tee coefficient and $K_{\text{branch}} = 2$ is the branch flow tee coefficient for threaded fittings. The factor of two is to account for the pressure drop at the stack inlet and outlet. $n_{\text{cells}}$ is the number of cells in the stack. In a typical VRFB piping system [14], the minor losses can be approximated by summing the losses at three elbows as well as the entrance and exit of the tank:

$$\Delta p_{\text{pipe,minor}} = 3 \times K_{\text{elbow}} \rho \frac{v_p^2}{2} + 2 \times K_{\text{tank}} \rho \frac{v_p^2}{2} \quad (31)$$

where $K_{\text{elbow}} = 1.5$ is the elbow friction coefficient, $K_{\text{tank}} = 0.97$ is the entry/exit loss coefficient and $v_p = Q/(\pi D_p^2/4)$ is the average electrolyte velocity in the pipe.

The total pressure loss in the VRFB system can then be obtained by

$$\Delta p_{\text{tot}} = \Delta p_{\text{stack,major}} + \Delta p_{\text{stack,minor}} + \Delta p_{\text{pipe,major}} + \Delta p_{\text{pipe,minor}} \quad (32)$$

and substituted into Eq. (26) to calculate the total pump power.

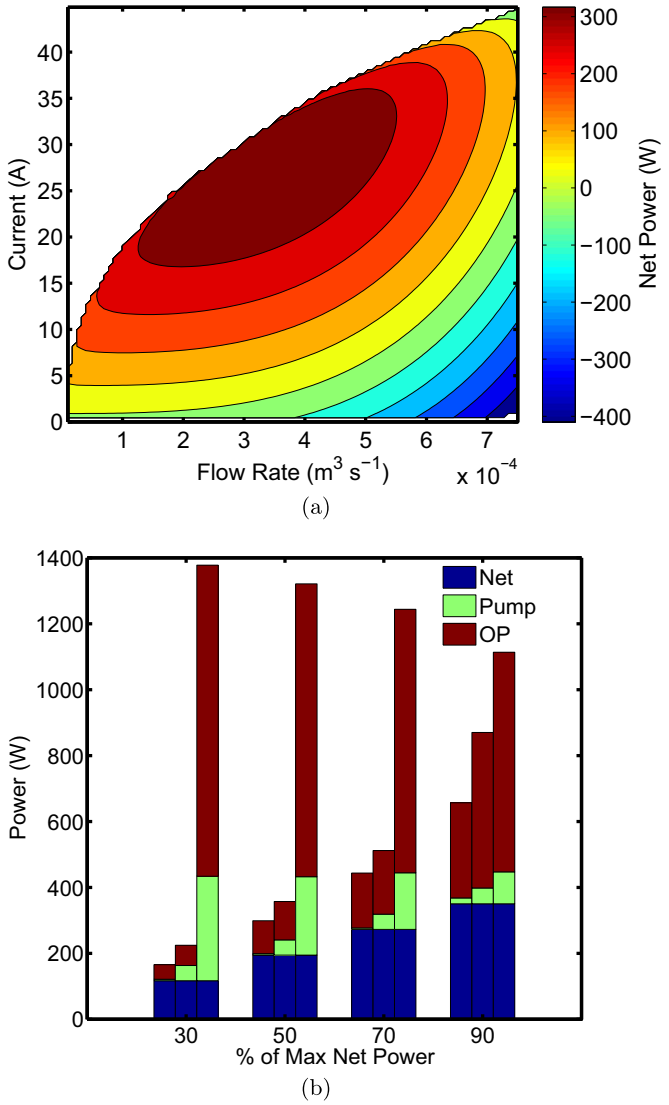


**Fig. 2.** (a) Net power over a range of operating points (flow rate and current) when $SOC_{\text{tank}}$ is 30%. (b) Net power and associated pumping and overpotential (OP) losses at three different operating points: Minimum current (left), flow rate is $3.5 \times 10^{-4}$ m$^3$ s$^{-1}$ and current is minimum necessary to reach given net power (middle), maximum current (right).

## 3. Results and discussion

Fig. 2a is a contour plot showing the net power as a function of current and flow rate when $SOC_{\text{tank}}$ is 30%. The pump power calculation is based on a 20 cell stack and the net power output is calculated using Eq. (1). The parameter values used for the simulations are provided in Table 1. At a given flow rate, the limiting current is governed by the rate of mass transfer of vanadium ions from the bulk solution to the electrode surface. As the current approaches the limiting current, the concentration overpotential increases significantly causing a sharp decrease in the net power. Consequently, the net power contour is cut off when the current exceeds 99% of the limiting current. Fig. 2a reveals that there are an infinite number of possible combinations of current and flow rate at a given $SOC_{\text{tank}}$ that yield a given net power (except the maximum net power, for which only one operating point is possible). Physical intuition suggests that the optimal operating point for maximizing battery life during discharge uses the minimum current necessary to provide the desired net power. The inherent advantages of operating at the minimum current operating point (MCOP) can be realized by noticing several distinct features in Fig. 2a. Although the MCOP requires slightly more pump power than the minimum flow rate operating point (MFOP) at a given net power, it would be more practical to run at the MCOP because the MFOP is much closer to the limiting current. Thus, the net power output at the MFOP would be very sensitive to changes in the operating point due to concentration overpotential effects. The plot also shows that the maximum net power occurs when the flow rate is about $3.5 \times 10^{-4}$ m$^3$ s$^{-1}$, meaning it would be futile to increase the flow rate further beyond this point.

Fig. 2b compares the net power and associated battery overpotential and pumping losses at three different operating points on Fig. 2a over a range of net power levels when $SOC_{\text{tank}}$ is 30%. Each group on the abscissa represents a net power level and each stack within a group corresponds to a different operating point used to

**Table 1**
Default parameter values used in the simulations.

| Parameter | Description | Value |
|---|---|---|
| $E_0^{\text{pos}}$ | Positive standard reduction potential | 1.004 V |
| $E_0^{\text{neg}}$ | Negative standard reduction potential | 0.26 V |
| $R$ | Gas constant | 8.3145 J mol$^{-1}$ K$^{-1}$ |
| $F$ | Faraday constant | 96845C mol$^{-1}$ |
| $A_m$ | Membrane area | 0.01 m$^2$ [17] |
| $c_{H^+}$ | Proton concentration | 4 M [17] |
| $w_m$ | Membrane width | $1.25 \times 10^{-4}$ m [17] |
| $w_e$ | Electrode width | $4 \times 10^{-3}$ m [17] |
| $w_c$ | Current collector width | $5 \times 10^{-3}$ m [17] |
| $\sigma_e$ | Electrolyte conductivity | 100 S m$^{-1}$ [17] |
| $\sigma_c$ | Current collector conductivity | $9.1 \times 10^4$ S m$^{-1}$ [17] |
| $\alpha$ | Charge transfer coefficient | 0.5 |
| $k_{\text{pos}}^{\text{ref}}$ | Positive reaction rate @ $T_{\text{ref}} = 293$ K | $1.2 \times 10^{-7}$ m s$^{-1}$ [23] |
| $k_{\text{neg}}^{\text{ref}}$ | Negative reaction rate @ $T_{\text{ref}} = 298$ K | $5.3 \times 10^{-6}$ m s$^{-1}$ [24] |
| $E_a$ | Activation energy | $52.4 \times 10^3$ J mol$^{-1}$ [23] |
| $L_p$ | Pipe length | 2 m [14] |
| $D_p$ | Pipe diameter | 0.03 m [14] |
| $\rho$ | Electrolyte density | 1400 kg m$^{-3}$ [14] |
| $\mu$ | Electrolyte dynamic viscosity | $4.928 \times 10^{-3}$ Pa s [15] |
| $L_e$ | Electrode length | 0.1 m [17] |
| $d_f$ | Mean fiber diameter | $1.76 \times 10^{-5}$ m [15] |
| $k_{KC}$ | Kozeny-Carmen constant | 4.28 [15] |

reach that net power. The stack on the left corresponds to the MCOP. The stack in the middle corresponds to an intermediate operating point where the flow rate is $3.5 \times 10^{-4}$ m$^3$ s$^{-1}$ and the current is the minimum necessary to reach the given net power. The stack on the right corresponds to the maximum current operating point, which is the worst possible operating point during discharge. This plot provides an illustrative means of analyzing the net power and associated losses at different operating points. At the MCOP, the flow rate is just high enough to overcome the sharp increase in concentration overpotential without excessive pump power. Consequently, a majority of the losses are due to overpotential, whereas the ratio of pumping loss to net power is negligible and barely visible in the plot. At the intermediate operating point, the flow rate is always higher than necessary to reach the desired net power, resulting in a greater ratio of pumping loss to net power. The maximum current operating point is distinctly the most inefficient of the three operating points as indicated by the significantly higher overpotential and pumping losses.

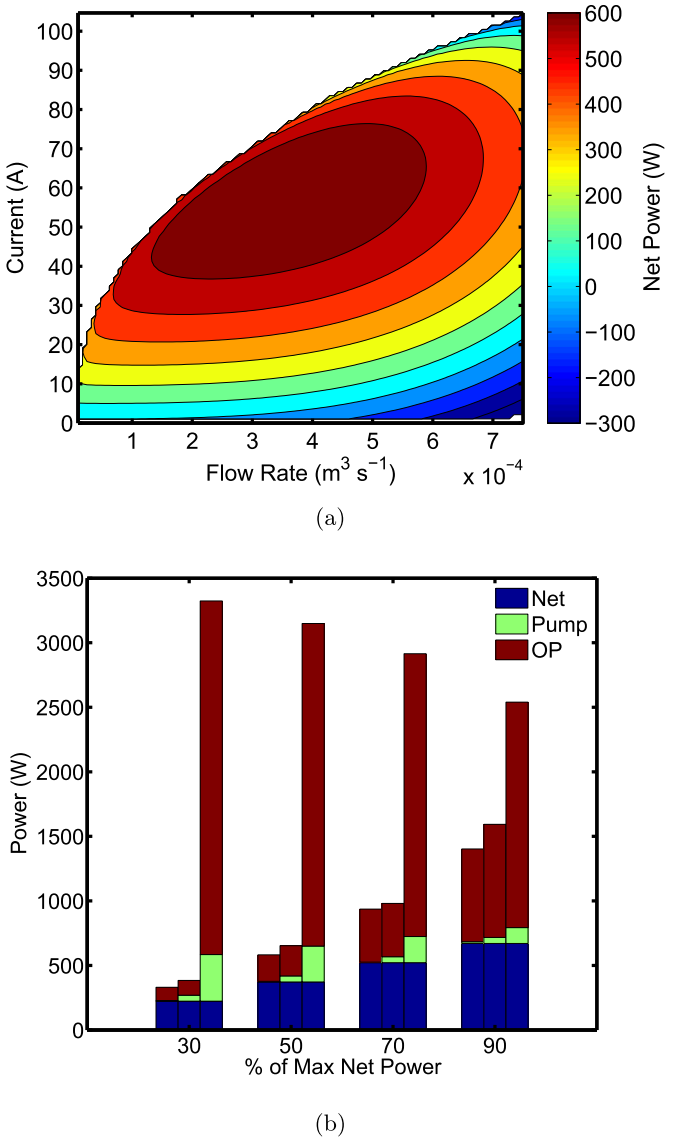


**Fig. 3.** (a) Net power over a range of operating points (flow rate and current) when $SOC_{tank}$ is 70%. (b) Net power and associated pumping and overpotential (OP) losses at three different operating points: Minimum current (left), flow rate is $3.5 \times 10^{-4}$ m$^3$ s$^{-1}$ and current is minimum necessary to reach given net power (middle), maximum current (right).

Fig. 3a and b are for the case when $SOC_{tank}$ is 70% and are analogous to Fig. 2a and b, respectively. When $SOC_{tank}$ is 70%, Fig. 3b shows that the ratio of pumping loss to net power is much lower than in the case when $SOC_{tank}$ is 30%. This occurs because a lower flow rate is needed to reduce the concentration overpotential in the cell when $SOC_{tank}$ is higher.

In the discussion so far, we have demonstrated a methodical and physics-based approach to devising an effective control strategy for a VRFB system. Assuming that an optimal control strategy was implemented, it was then straightforward to analyze the upper efficiency limits of a given VRFB system design by comparing the net power to the associated overpotential and pumping losses. In the next part of this section, we extend the analysis by showing how the maximum net power of a VRFB system running optimally is affected by varying important design parameters including electrode porosity, stack temperature, and vanadium concentration. During the initial design stage, this insight can be helpful for sizing the VRFB system appropriately to handle the intended power requirements while reducing capital costs.

Fig. 4 shows the maximum net power and the corresponding current and flow rate control inputs for $SOC_{tank}$ from 10 to 90% with electrode porosities of 0.93, 0.8, and 0.68. This range of electrode porosities has been used in numerous research studies and pilot experiments [5–8,15]. As electrode porosity increases, the maximum net power increases. This trend can be explained by Eq. (27), which predicts that head loss in the electrode decreases with increasing porosity. Therefore with higher porosity, the pump consumes less power at a given flow rate and the limiting current can be increased further. In the case of $\varepsilon = 0.93$ when $SOC_{tank}$ is high, the peak power is achieved at a slightly lower flow rate compared to when $SOC_{tank}$ is 50%. This phenomenon can be explained by Eq. (11), which predicts that the minimum activation overpotential occurs when $SOC_{cell}$ is 50%. Using a lower flow rate not only decreases the pump power, but also makes the average

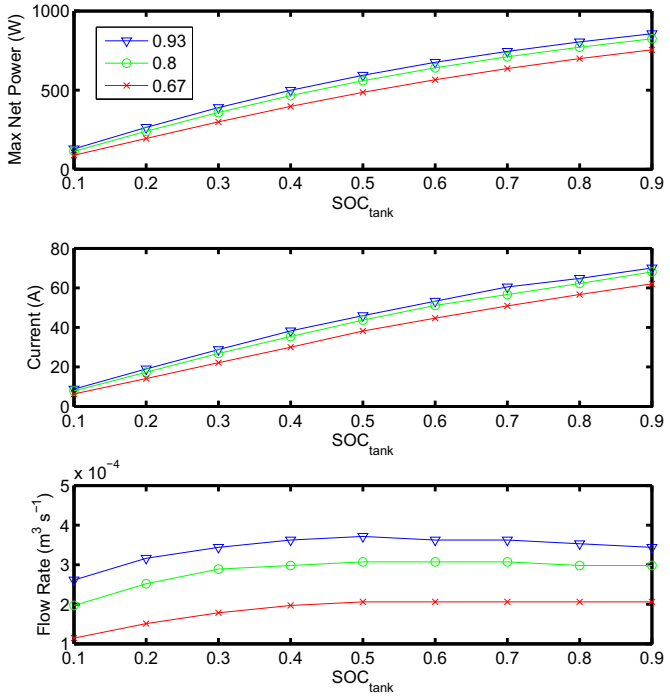


**Fig. 4.** Maximum net power (top) and the corresponding current (middle) and flow rate (bottom) control inputs for $SOC_{tank}$ from 10 to 90% with electrode porosities of 0.93, 0.8, and 0.68.

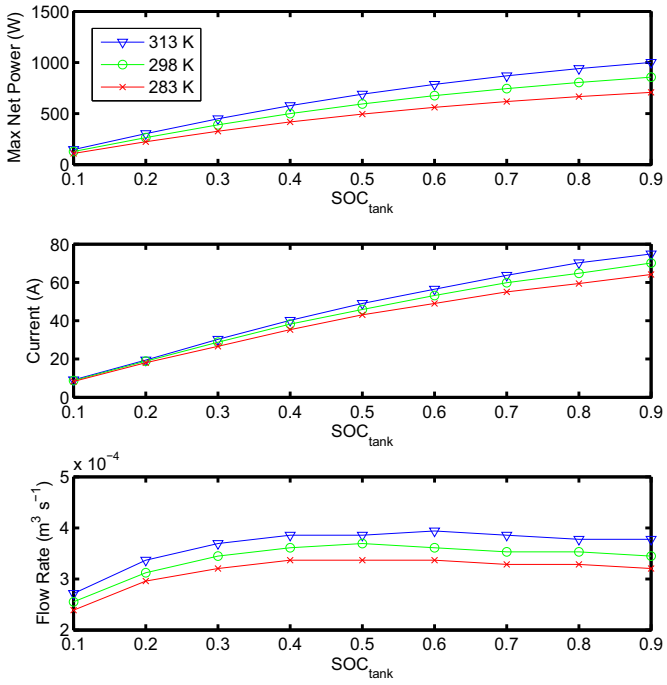


**Fig. 5.** Maximum net power (top) and the corresponding current (middle) and flow rate (bottom) control inputs for $SOC_{tank}$ from 10 to 90% with stack temperatures of 313 K, 298 K, and 283 K.

SOC in the cell closer to 50% when $SOC_{tank}$ is high. However, the trade-off is that decreasing the flow rate also lowers the mass transfer coefficient and therefore the limiting current. That could likely explain why the same trend is not apparent in the case of $\varepsilon = 0.8$ or 0.68, where the peak power is achieved at a relatively constant flow rate when $SOC_{tank}$ is high.

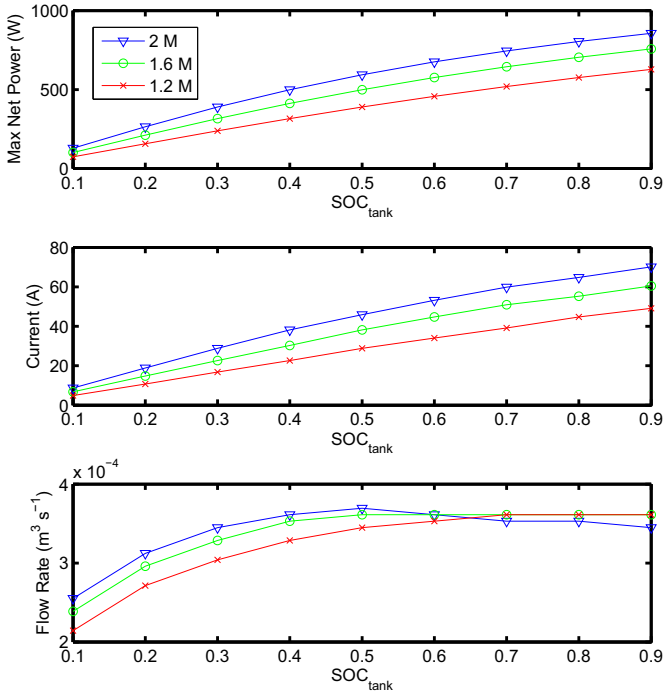


**Fig. 6.** Maximum net power (top) and the corresponding current (middle) and flow rate (bottom) control inputs for $SOC_{tank}$ from 10 to 90% with total vanadium concentrations of 2 M, 1.6 M, and 1.2 M.

Fig. 5 shows the maximum net power and the corresponding current and flow rate control inputs for $SOC_{tank}$ from 10 to 90% with stack temperatures of 318 K, 298 K, and 278 K. In all cases, the electrode porosity is 0.93 and the total vanadium concentration is 2 M. At higher temperatures, the increase in maximum net power can be attributed to the decrease in activation overpotential according to Eqs. (11) and (14). Although increasing the stack temperature increases the peak power, laboratory studies report that vanadium begins to precipitate beyond 40 °C [14]. These results can be helpful in evaluating the necessity and determining the required capabilities of a temperature regulation system based on the climate of the deployment location.

Fig. 6 shows the maximum net power and the corresponding current and flow rate control inputs for $SOC_{tank}$ from 10 to 90% with total vanadium concentrations of 2 M, 1.6 M, and 1.2 M. In all cases, the electrode porosity is 0.93 and the stack temperature is 298 K. The maximum net power evidently increases with a higher total vanadium concentration. However, the flow rate required to achieve maximum power decreases when $SOC_{tank}$ is above 50% for 2 M vanadium concentration, whereas the flow rate remains relatively constant for the 1.6 M and 1.2 M cases. With a lower total vanadium concentration, a higher flow rate is required to keep the average cell overpotential low. Depending on the total vanadium concentration being used, it can be important to consider the flow rate strategy when trying to take full advantage of the peak power when $SOC_{tank}$ is high.

## 4. Conclusions

In this paper, we developed a physics-based model incorporating battery overpotential and pumping losses that can be used as a valuable tool for optimizing the design and control of a stack level VRFB system. Sufficient detail was included in the overpotential model to account for the effects of flow rate on the limiting current and on the non-uniform vanadium concentration in the cell. Therefore, system performance can be predicted accurately even at high current densities. First we used the model to devise a control strategy that maximizes battery life during discharge. Assuming the optimal control strategy was implemented, we then determined the upper efficiency limit of a given VRFB system at different SOC and net power levels. The net power and associated overpotential and pumping losses were also compared quantitatively at different operating points. Furthermore, we investigated the effects of varying the electrode porosity, stack temperature, and total vanadium concentration on the peak power output for $SOC_{tank}$ from 10 to 90%. For a certain combination of VRFB system design parameters, we found that a non-intuitive flow rate strategy should be followed to take full advantage of the peak power available when $SOC_{tank}$ is high. The methodology and analysis demonstrated in this paper can readily be adapted to optimize other critical parameters in the design process and help to further reduce capital costs.

## Acknowledgments

This research was supported by National Science Foundation (NSF)-Control Systems Program CAREER Award CMMI-1056020.

## References

[1] M. Skyllas-Kazacos, M.H. Chakrabarti, S.A. Hajimolana, F.S. Mjalli, M. Saleem, J. Electrochem. Soc. 158 (2011) R55–R79.
[2] E.H. Mouron, University of Tennessee Honors Thesis Projects, 2011.
[3] B. Sun, M. Skyllas-Kazacos, Electrochim. Acta 37 (1992) 1253–1260.
[4] Q.H. Liu, G.M. Grim, A.B. Papandrew, A. Turhan, T.A. Zawodzinski, M.M. Mench, J. Electrochem. Soc. 159 (2012) A1246–A1252.
[5] A. Shah, M. Watt-Smith, F. Walsh, Electrochim. Acta 53 (2008) 8087–8100.

[6] H. Al-Fetlawi, A. Shah, F. Walsh, Electrochim. Acta 55 (2009) 78–89.
[7] H. Al-Fetlawi, A. Shah, F. Walsh, Electrochim. Acta 55 (2010) 3192–3205.
[8] A. Shah, H. Al-Fetlawi, F. Walsh, Electrochim. Acta 55 (2010) 1125–1139.
[9] Q. Xu, T.S. Zhao, P.K. Leung, Appl. Energy 105 (2013) 47–56.
[10] G. Kear, A.A. Shah, F.C. Walsh, Int. J. Energy Res. 36 (2012) 1105–1120.
[11] E. Hittinger, J. Whitacre, J. Apt, J. Power Sources 206 (2012) 436–449.
[12] D.S. Aaron, Q. Liu, Z. Tang, G.M. Grim, A.B. Papandrew, A. Turhan, T.A. Zawodzinski, M.M. Mench, J. Power Sources 206 (2012) 450–453.
[13] X. Ma, H. Zhang, C. Sun, Y. Zou, T. Zhang, J. Power Sources 203 (2012) 153–158.
[14] B. Xiong, J. Zhao, K. Tseng, M. Skyllas-Kazacos, T.M. Lim, Y. Zhang, J. Power Sources 242 (2013) 314–324.
[15] D. You, H. Zhang, J. Chen, Electrochim. Acta 54 (2009) 6827–6836.
[16] H.W. Bindner, C. Krog Ekman, O. Gehrke, F.R. Isleifsson, Characterization of Vanadium Flow Battery, Danmarks Tekniske Universitet, Risø Nationallaboratoriet for Bæredygtig Energi, 2010.
[17] A.A. Shah, R. Tangirala, R. Singh, R.G.A. Wills, F.C. Walsh, J. Electrochem. Soc. 158 (2011) A671–A677.
[18] T.E. Springer, J. Electrochem. Soc. 138 (1991) 2334–2342.
[19] A. Bard, L. Faulkner, Electrochemical Methods: Fundamentals and Applications, Wiley, 2000.
[20] D. Schmal, J.V. Erkel, P.J.V. Duin, J. Appl. Electrochem 16 (1986) 422–430.
[21] P.V. Kokotovic, J. O'Reilly, H.K. Khalil, Singular Perturbation Methods in Control: Analysis and Design, Academic Press, Inc., Orlando, FL, USA, 1986.
[22] C.L. Chen, H.K. Yeoh, M.H. Chakrabarti, Electrochim. Acta 120 (2014) 167–179.
[23] H. Liu, Q. Xu, C. Yan, Y. Cao, Y. Qiao, et al., Int. J. Electrochem. Sci. 6 (2011) 3483–3496.
[24] T. Yamamura, N. Watanabe, T. Yano, Y. Shiokawa, J. Electrochem. Soc. 152 (2005) A830–A836.